Coevolutionary optimization of a fuzzy logic controller for Antilock Braking Systems under changing road conditions

Javier Pérez Fernández, *Graduate Student Member, IEEE*, Manuel Alcázar Vargas, *Student Member, IEEE*, Juan M. Velasco García, *Student Member, IEEE*, Juan A. Cabrera Carrillo and Juan J. Castillo Aguilar, *Member, IEEE*

***Abstract*— An anti-lock brake system based on fuzzy logic has been developed and optimized to cope with changes in adherence road conditions. Conventional control systems have to be tuned by conducting simulations and tests on different surfaces before putting them into use. This way, large amounts of computational and testing times are required. The main objective of this work is to propose a methodology to simplify the process of obtaining a controller for antilock brake systems through a combination of optimization and simulation. To this end, an evolutionary algorithm based on the coevolution of two species has been used to tune the proposed fuzzy logic controller. The controller evolves competitively with the environment to optimize its response to different adherence conditions. Finally, the optimized controller has been implemented in a real motorcycle to compare its performance with a conventional system.**

***Index Terms*— Coevolutionary, Genetic algorithms, Fuzzy Logic Controller (FLC), Antilock Brake System (ABS), Vehicle safety.**

I. Introduction

The anti-lock brake system (ABS) is one of the major advances in active safety in vehicles. It reduces the braking distance and ensures the maneuverability of the vehicle during emergency situations by preventing the wheels from locking during braking [1][2].

Research groups have devoted big efforts to the design of brake system controllers that minimize the braking distance while avoiding the locking of the wheels. The first control logics used state machines based on the slip ratio, road condition and wheel angular acceleration while avoiding the estimation of forces. The aforementioned logics did not use continuous pressure control [1]. Currently, controllers with continuous pressure control are used, such as: proportional integral derivative (PID) [3][4], fuzzy logic [5], sliding mode control (SMC) [6][7], neural networks [8] and even controllers that do not require slip or adhesion knowledge [9][10].

Meeting real-time requirements and having the flexibility to adapt to different vehicles and road conditions makes it difficult to choose the control logic. This is why fuzzy logic-based controllers are widely used in ABS controls as they have a parallel structure that reduces the delays without the need to execute an adaptive control law or complex mathematical computations. The use of fuzzy logic in combination with other controllers is a suitable candidate for the implementation of ABS controls. Controllers such as PID [11][12], SMC[13], adaptive control [14] or adaptative SMC [15][16][17] have been proposed. However, these approaches do not make use of the inherent parallelism and simplicity of fuzzy logic controllers (FLC). It also provides flexibility without losing understanding, unlike neural networks [8][18] where, once trained, we face a "black box".

Most of these research papers test the performance of the proposed controllers by means of simulations or using test benches. However, they are not tested in real conditions. Besides, the tire models used do not fully reproduce real tire behavior and simulation models do not include the temporal response of actuators and brake system components and the delays in measurement systems and estimation algorithms. This way, often, when these controllers are tested in real conditions, fluctuations in the response and poor performance are observed.

This paper proposes the use of an FLC to optimize the longitudinal braking process of a two-wheeled vehicle. Contrary to other approaches, in which a quarter or half-vehicle model is considered, a full multibody vehicle model implemented in Bikesim® and Simulink® is used. This model takes into account the load transfer of the vehicle during the braking process, the transient effects that occur in the generation of contact forces as well as delays in the response of the components of the hydraulics of the braking system.

Since the most commonly used tire models [19][20] are typically stationary, a transient term should be introduced to reproduce the dynamic behavior of the tires.

The key contribution of this work is the optimization of the FLC. Rules and membership functions (MFs) are optimized to modify the control surface according to the dynamics of the tire-road contact. Although through linguistic rules knowledge-based systems [21] can be transferred to diffuse systems, transferring knowledge without losing information entails a great difficulty [22][23][24][25]. Moreover, it does not provide the certainty that the proposed FLC will perform properly in changing road conditions. A priori, the optimization of an FLC

This work was partly supported by the Ministry of Economy, Industry and Competitiveness under grant TRA2015-67920-R, partly by the Ministry of Education, Culture and Sport under grant FPU17/03161, and partly by the University of Málaga.

(Corresponding author: Javier Pérez Fernández)

The authors are with the Mechanical Engineering Department, University of Málaga, 29071 Málaga, Spain (e-mail: javierperez@uma.es , manuel.alcazar@uma.es , juanmav@uma.es , jcabrera@uma.es , juancas@uma.es)

in different road conditions requires a high computational cost. An optimization based on genetic algorithms [26][27] or particle swarm [28][29] requires testing possible road conditions and surface changes in each iteration. In order to reduce the number of combinations to be simulated during the optimization process, the use of a coevolutionary algorithm is proposed.

Coevolution describes the evolution between two or more species that interact with each other. They can be grouped according to their behavior as: antagonists/competitive [30] (prey and predator), symbiotic/cooperative [31][32] or mutual exploitation/non-symmetric [33] (host and parasite). In [34][35] using coevolution between competitive species to solve engineering problems is proposed. Unlike other approaches where this process of coevolution is applied to a set of data [36], this paper optimizes the control logic by simulating different road conditions.

In this approach, the controllers are optimized against different environments. The controller (prey) evolves against different environments (predator) to improve braking performance. The algorithm focuses on the optimization where the controller has worse results avoiding the repetition of the optimization in environments where it already obtained a good result. This avoids simulating all road conditions in each iteration, thus reducing the number of total simulations in comparison with a simple genetic algorithm [37]. This process of coevolution between both species is repeated iteratively until the controller obtained behaves properly in different road conditions.

The performance of the controller is evaluated by means of simulations and real tests using a 35 kW two-wheel electric vehicle equipped with the necessary sensors for this purpose. To this end, estimation and optimization algorithms were developed and integrated into an embedded system in the vehicle's control electronics.

The main contributions of this paper are the following:

- the development of a new control algorithm optimization strategy based on coevolution to reduce the optimization time.
- to take into account the delays in the temporal response of the brake system components in the simulations carried out to test the performance of the controllers. This way, the controllers are easily transferred to real applications.

This work is structured as follows: system definition and models are described in section II. Section III is devoted to the slip and road condition estimation by using a Kalman filter. Section IV presents the fuzzy logic ABS controller. Next, the coevolutionary FLC optimization is described in Section V. Simulation, experimental results and discussions are shown in Section VI. Finally, conclusions are drawn in Section VII.

II. System definition and modeling

Vehicle models have to reproduce real systems with sufficient detail to ensure their subsequent validation. BikeSim® software has been used to model the dynamic behavior of the motorcycle. Besides, the multibody model of the motorcycle is solved by means of this software, while the dynamics of tire-road contact as well as the braking system are modeled independently using Simulink®.This way, the dynamics and response times of the whole system are taken into account.

The overall behavior of the controller is affected by the delays of the brake system components and measurements. These delays have to be taken into account in the design phase of ABS controllers. A common lack in the majority of proposed ABS controller optimization methods is not including these delays in the models used in the simulations. Although this makes the mathematical model much more stable, it provides results that do not fit in with reality. Thus, they lead to ABS controllers that have no oscillations in simulations, even on high adherence roads where system delays have a big influence. As a result, the performance of these controllers is poor when they are tested in real vehicles. For this reason, the dynamics of these systems are taken into account in this work in order to develop controllers that work efficiently in real vehicles without requiring further refinements.

A. Tire Model

The dynamics of the vehicle to be controlled during the braking process is determined by the contact between the tire and the road. The longitudinal force (1), according to tire-road contact models [19][20], depends on the slip (κ) (2) and the road condition (λ_{μ_x}). To determine both parameters, it is necessary to measure or estimate the speed of the vehicle (V_x) and the wheels ($R_e\omega$) as well as the forces appearing in the contact: vertical force (F_z) and longitudinal force (F_x).

$$F_x = \mu_x(\kappa, \lambda_{\mu_x})\, F_z \tag{1}$$

$$\kappa = \frac{-V_{sx}}{|V_x|} = \frac{R_e\omega - V_x}{|V_x|} \tag{2}$$

In this paper, Pacejka's magic formula [19] is used to model tire behaviour. This model contemplates a non-linear relationship between the slip and the longitudinal force (3). The parameters of the empirical equation of the steady-state tire-road contact model are obtained by testing the tire on test benches.

$$F_x = D_x \sin\left[C_x \arctan\left\{B_x\kappa - E_x(B_x\kappa - \arctan(B_x\kappa))\right\}\right] \tag{3}$$

$$\begin{cases} D_x = \lambda_{\mu x} F_z P_{D_x}(df_z) \\ C_x = P_{C_x}(df_z) \\ B_x = \frac{P_{B_x}(df_z)}{\lambda_{\mu x}} \\ E_x = P_{E_x}(df_z) \end{cases} \tag{4}$$

$$df_z = \frac{Fz - F_{z0}}{F_{z0}} \tag{5}$$

Where ($P_{Bx}, P_{Cx}, P_{Dx}, P_{Ex}$) (4) are polynomial functions whose coefficients are fitted from data gathered in experimental tests on the tire test bench. Finally, df_z (5) is the normalized change in vertical load.

The curves of the tire adhesion coefficient (Fig.1) show the steady-state behavior using the parameters obtained by Sharp [38]. It is observed that, according to the slip ratio (κ) (2), the system is stable depending on whether it is to the left or right of the maximum adhesion value for each road.

ABS tries to keep the slip around the value that provides the maximum grip (dashed line) to reduce the brake distance as much as possible. It also allows maintaining a slip ratio that ensures vehicle maneuverability. This optimum slip ratio is

affected by the road condition and increases as the grip of the road increases.

Remark 1: Pacejka's magic formula is a standard method widely used in vehicle dynamics studies [39][40][41] and throughout industry to describe the tire-road interaction at the contact patch. This empirical model can reproduce the tire-road interaction accurately enough without requiring great computational time. These two characteristics make this model very appropriate to be used in control algorithms.

B. *Tire Transient Model*

The previous model, despite its non-linearity, does not reproduce transient tire behavior adequately. Due to the fact that during the braking process the slip changes quickly, transient effects have to be taken into account in the modelling of the tire-road interaction. For this purpose, a first-order differential equation (6) is introduced [19] to substitute the measured slip (κ) by a delayed slip (κ') (7), reproducing this way the delay between the slip and the generation of the corresponding force.

$$\sigma_\kappa \frac{d\kappa'}{dt} + |V_x|\kappa' = \sigma_\kappa \dot{\kappa'} + |V_x|\kappa' = -V_{sx} \tag{6}$$

$$\tau_\kappa \frac{d\kappa'}{dt} + \kappa' = \tau_\kappa \dot{\kappa'} + \kappa' = \kappa \tag{7}$$

$$\tau_\kappa = \frac{\sigma_\kappa}{|V_x|} \tag{8}$$

Where (σ_κ) is the relaxation length, which is defined as the distance the tire travels to generate 63% of the total force. τ_κ is the rise time (8) associated to the change, which depends on the relaxation length and vehicle speed.

C. *Friction Brake Model*

The dynamic response of the braking system components also affects the performance of the ABS controller. For this purpose, the response time of the subsystems has to be taken into account. Otherwise, simulation results will not reproduce reality properly.

The diagram of the brake-by-wire system used is described in Fig. 2. It consists of a brake pump, brake disc and pads. The brake pump generates brake pressure by means of an electric motor and a worm gear.The response of the hydraulic pump is modeled as a DC motor according to (9). This equation provides the electric motor torque output (T_e) as a function of the input voltage (V):

$$LK_t^{-1} \frac{dT_e(t)}{dt} + RK_t^{-1} T_e(t) = V(t) - K_m \dot{\theta} \tag{9}$$

Where K_t is the torque constant, R is the internal resistance of the winding, L is the rotor inductance, K_m is the electromotive force constant and $\dot{\theta}$ is the motor speed. Due to the reduced piston displacement, motor speed is assumed to be null. A first-order system is used to model the hydraulic system response. The asymmetrical behavior of the piston and the brake pads in contact with the disc makes it necessary to use different time constants to reproduce pressure increases (τ_{up}) or decreases (τ_{down}) (10).

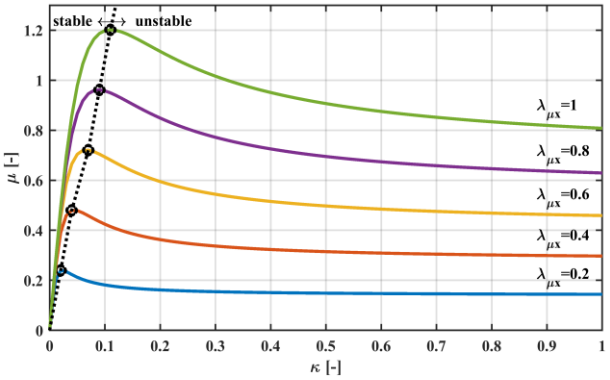

Fig. 1. Tire slip-adhesion steady-state curve for different road conditions

$$K_{\frac{Nm}{Bar}} T_e(t) = \begin{cases} \tau_{down} \frac{dT_b(t)}{dt} + T_b(t), \frac{dT_b(t)}{dt} < 0 \\ \tau_{up} \frac{dT_b(t)}{dt} + T_b(t), \frac{dT_b(t)}{dt} \geq 0 \end{cases} \tag{10}$$

$$K_{Nm/Bar} = \mathrm{S_p}\, \mu_\mathrm{p}\, \phi_d \tag{11}$$

Constant $K_{Nm/Bar}$ relates the pressure of the hydraulic system to the braking torque (T_b) in the wheel. It is the product of the piston area ($\mathrm{S_p}$), the friction coefficient of the brake pad (μ_p) and the brake disc diameter (ϕ_d) (11).

D. *Measurement Delay*

Vehicle control system performances are deterioriated by measurement time delays and poor sensor resolutions. Both factors affect the controllability of the system and should be included in the simulation models. In particular, the measurement of pressure and speed in a vehicle have a major influence during the braking process. Since pressure sensors are costly, many manufacturers do not install them or decide to use low-cost sensors with lower resolution. To reproduce this fact, a ±1bar sensor resolution has been simulated.

The measurement of wheel speeds is carried out by means of incremental encoders installed in each wheel. These sensors generate a signal with a frequency proportional to the wheel rotational speed. At high speeds, this low-cost technology has a very good resolution, but its resolution is poor at low speed. In addition, they require more filtering, causing a measurement delay of around 10 ms. This delay increases up to 25 ms when performing the derivative to obtain the angular accelerations. In extreme braking conditions, the locking of the wheels takes place at around 150-200 ms after full pressure has been applied. Therefore, for the simulation results to be valid, it is necessary to take into account the delays in the measurement of wheel speed.

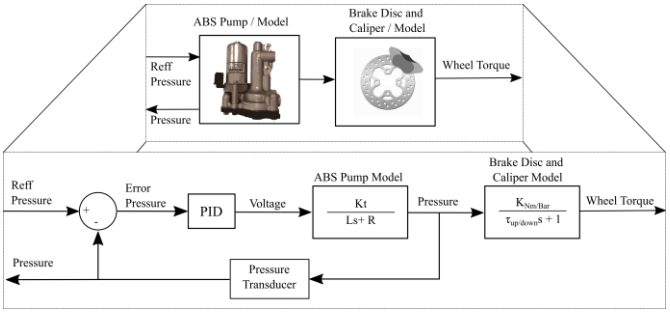

Fig. 2. Brake by-wire system architecture (brake pump, brake disc and pads)

Remark 2: Although this paper is not focused on developing a new vehicle model, it seeks to highlight the importance of the proper modeling of vehicle components response. This way, the controller obtained after the optimization process will be used in the real vehicle without requiring a further major tuning process.

III. Slip and Road Condition Extended Kalman Filter (EKF) Estimator

Slip (κ) and road condition ($\lambda_{\mu x}$), as presented in the previous section, are key parameters to perform the grip control required by ABS. In a real vehicle, both parameters are difficult to measure. The slip requires the measurement of the vehicle's speed (V_x). This cannot be obtained by GPS devices due to their poor latency. Hence, an estimation algorithm provides a clear advantage over installing expensive speed measurement devices in vehicles. On the other hand, road condition can only be known if contact forces in the tire are measured. This can be done by using a dynamometric rim, but these devices are not installed in vehicles due to its extremely high cost. Therefore, tire contact forces also need to be estimated. The use of a double Kalman structure [42][43] is proposed in this work, in which the first filter estimates the interaction forces between the tire and the road while the second one estimates the road condition using data provided by the first one. This estimation process is carried out in two stages to ensure convergence of the estimated variables. This is achieved by decoupling the non-linear equations that reproduce tire behaviour. This way, the accuracy of the estimation of the road condition is assured, obtaining a robust system that can cope with errors in the measurements [44][45].

A. Speed and forces estimator

A simple dynamic model that reproduces a vehicle's response is needed to perform real-time estimation. In this work, a planar model of a two-wheeled vehicle with the characteristics of the real vehicle is used.

Fig. 3 shows the forces that appear during the braking of the vehicle with both wheels. Table I shows the parameters used in the model. The dynamic equilibrium leads to the equations that model the horizontal (12) and vertical movements (13), pitch of the chassis (14) and rotation of the front (15) and rear wheels (16). A simplified suspension model is used to calculate the vertical coordinate position (z). This model takes into account the equivalent stiffness and damping to obtain the height of the center of gravity by knowing its accelerations and angular velocities (17) (18).

$$Ma_x = M(\ddot{x} + \dot{\theta}V_z) = F_{xr} + F_{xf} + C_d\,V_x^2 \quad (12)$$
$$Ma_z = M(\ddot{z} + \dot{\theta}V_x + g) = F_{zr} + F_{zf} \quad (13)$$
$$I_y\ddot{\theta} = -F_{zf}L_f + F_{zr}L_r - F_{xf}z - F_{xr}z \quad (14)$$
$$I_{wf}\dot{\omega}_f = T_{bf} - F_{xf}R_f \quad (15)$$
$$I_{wr}\dot{\omega}_r = T_{br} - F_{xr}R_r \quad (16)$$
$$F_{zf} = -k_f\big(z - L_0 - L_f\theta\big) - C_f(\dot{z} - L_f\dot{\theta}) \quad (17)$$
$$F_{zr} = -k_r(z - L_0 + L_r\theta) - C_f(\dot{z} + L_r\dot{\theta}) \quad (18)$$

An extended Kalman filter is proposed to estimate the forces and velocities using nonlinear equations (12-18). The state

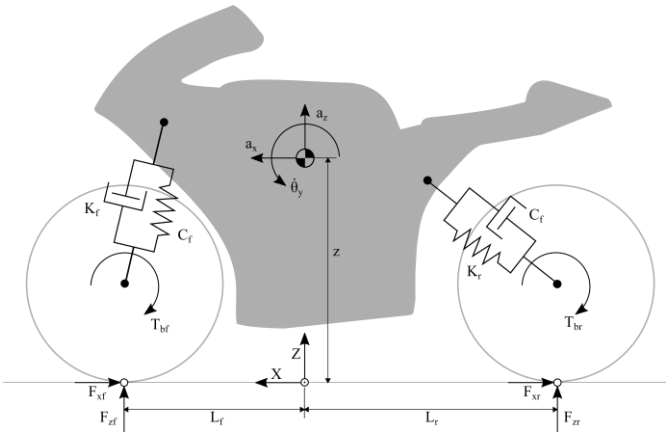

Fig. 3. Planar motorcycle model

vector (x_k) (19) includes tyre vertical forces (F_{zf}, F_{zr}), horizontal forces (F_{xf}, F_{xr}) and vehicle speed (V_x). The measurement vector (j_k) (20) consists of the variables obtained through the sensors installed in the motorcycle. An inertial measurement unit (IMU) is used to obtain horizontal (a_x) and vertical (a_z) accelerations, a gyro for angular acceleration ($\ddot{\theta}$) and pressure transducers in the pressure circuit to determine the braking torque in the front (T_{bf}) and rear wheel (T_{br}).

$$x_k = \left[F_{xf}, F_{xr}, F_{zf}, F_{zr}, V_x\ \right]^T \quad (19)$$
$$j_k = \left[a_x, a_z, \ddot{\theta}, T_{bf}, T_{br}\right]^T \quad (20)$$

System dynamics model equations (21) and measurement model equations (22) relate current states ($_k$) with previous states ($_{k-1}$) and measurements respectively.

State variables and measured variables are disturbed by white noise with a zero mean and standard deviation Q and R, respectively. Where u_{k-1} and v_k represent the noise of the model and the measures respectively.

$$x_k = \phi_{k-1}(x_{k-1}) + u_{k-1} \quad (21)$$
$$j_k = h_k(x_k) + v_k \quad (22)$$

A first-order random walk is used to estimate the forces. Equation (12), which models vehicle longitudinal dynamics, is required to estimate vehicle velocity (23):

$$\phi_{k-1}(x_{k-1}) = \begin{bmatrix} F_{xf}(k-1) \\ F_{xr}(k-1) \\ F_{zf}(k-1) \\ F_{zf}(k-1) \\ v_x(k-1) + \Delta t\left(\frac{F_{xr}(k-1)+F_{xf}(k-1)+C_d\,v_x^2(k-1)}{M} - \dot{\theta}V_z\right) \end{bmatrix} \quad (23)$$

Where pitch rate ($\dot{\theta}$) and vertical speed (V_z) are obtained by integrating pitch acceleration ($\ddot{\theta}$) and vertical acceleration (a_z) respectively.

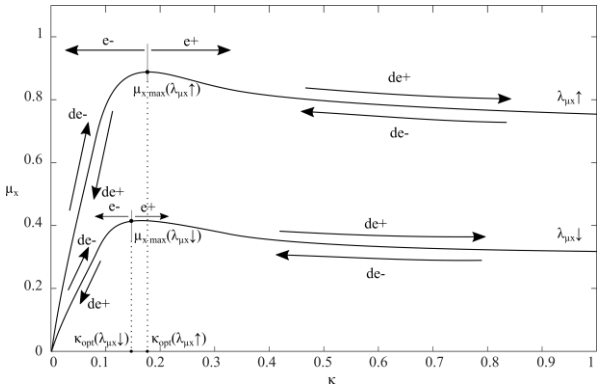

Fig. 4. Coefficient of adhesion (μ_x) of the tire in relation to slip (κ) for two different roads ($\lambda_{\mu x}$).

$$h_k(x_k) = \begin{bmatrix} \frac{F_{xr}(k)+F_{xf}(k)+C\,V_x^2(k)}{M} \\ \frac{F_{zf}(k)+F_{zr}(k)}{M} \\ \frac{-F_{zf}(k)L_f+F_{zr}(k)L_r-F_{xf}(k)z-F_{xr}(k)z}{I_y} \\ I_{wf}\dot{\omega}_f + F_{xf}(k)R_f \\ I_{wr}\dot{\omega}_r + F_{xr}(k)R_r \end{bmatrix} \quad (24)$$

The relationship between state variables and measured variables (24) is obtained from the equations that model vehicle dynamics (12-18). The angular accelerations ($\dot{\omega}_f, \dot{\omega}_r$) of the wheels are obtained by deriving the angular speed obtained from the sensors installed in the wheels.

B. Road condition estimator

The second Kalman filter uses a simplified model (25) of tyre dynamics (3) that does not consider the coefficients associated with parameter (df_z) to estimate the road condition, thus requiring lower computational cost.

$$F_x = \lambda_{\mu x} F_z\, P_{D_{x1}} \sin\left[P_{C_{x1}} \arctan\left\{\frac{P_{B_{x1}}}{\lambda_{\mu x}\, P_{C_{x1}}\, P_{D_{x1}}}\kappa'\right\}\right] \quad (25)$$

Where ($P_{Bx1}, P_{Cx1}, P_{Dx1}, P_{Ex1}$), are the independent terms of the polynomial functions ($P_{Bx}, P_{Cx}, P_{Dx}, P_{Ex}$) obtained by empirical tests.

In this case, the state vector (26) is the road condition ($\lambda_{\mu x}$). The measurement vector is the horizontal force (27), which was obtained in the first EKF. The rear wheel is used to estimate the road condition.

$$x_k = \left[\lambda_{\mu x}\right]^T \quad (26)$$

$$j_k = [F_{xr}]^T \quad (27)$$

The temporal evolution of the state variable (28) is again modelled with a random walk. Measurement equation (29) is obtained from the simplified tire model described above.

$$\phi_{k-1}(x_{k-1}) = \left[\lambda_{\mu x}(k-1)\right] \quad (28)$$

$$h_k(x_k) = \lambda_{\mu x}(k-1) F_{zr}\, P_{D_{x1}} \sin\left[P_{C_{x1}} \arctan\left\{\frac{P_{B_{x1}}}{\lambda_{\mu x}\,(k-1) P_{C_{x1}}\, P_{D_{x1}}}\kappa'\right\}\right] \quad (29)$$

TABLE I
MOTORCYCLE MODEL PARAMETERS

Symbol	Description	Symbol	Description
x	Longitudinal displacement (CoG)	I_y	Moment of inertia around the Y axis
z	Vertical displacement (CoG)	I_{wf}	Front wheel spin inertia
V_x	Longitudinal speed	I_{wr}	Rear wheel spin inertia
V_z	Vertical speed	K_f	Front suspension stiffness
M	Mass	K_r	Rear suspension stiffness
a_x	Longitudinal acceleration	C_r	Front suspension damping
a_z	Vertical acceleration	C_f	Rear suspension damping
θ	Pitch angle	L_0	Stiffness preload
R_f	Front tire radius	C_d	Drag coefficient
R_r	Rear tire radius	T_{bf}	Brake torque front tire
L_f	Front half length	T_{br}	Brake torque rear tire
L_r	Rear half length	F_{xf}	Pitch angle
ω_f	Front angular wheel speed	F_{xr}	Brake torque front tire
ω_r	Rear angular wheel speed	F_{zf}	Brake torque rear tire

Remark 3: Several methods, such as sliding mode observers, moving horizon estimation, Kalman filter and particle filter-based methods, can be used to perform parameter estimation. Among them, the Extended Kalman filter is widely used to estimate the states in dynamic systems [42][43][44][45]. In this paper, EKF is used as a tool to estimate vehicle states due to its good compromise between accuracy and computational cost.

IV. FUZZY LOGIC ANTILOCK BRAKE SYSTEM CONTROLLER

To control the dynamics of the tire while the braking process is in progress, the tire states have to be known a priori to be able to determine the optimal braking pressure. For this purpose, the inputs (x_1, x_2, x_3) and output (y_1) used for the design of the FLC are defined. Inputs are defined taking into account the adherence curve (Fig. 4). The main task of the controller is to prevent wheels from locking ($\kappa = 1$) and to maximize grip. Avoiding locking is not difficult if wheel speeds are correctly measured. However, other parametes are required to make it possible for the controller to work close to the optimum level of slip.

$$x_1 = e = \kappa' - \kappa'_{opt} \quad (30)$$

$$x_2 = de = \frac{d\kappa'}{dt} - \frac{d\kappa'_{opt}}{dt} = \dot{\kappa}' - \dot{\kappa}'_{opt} \quad (31)$$

$$x_3 = \lambda_{\mu x} \quad (32)$$

$$\kappa'_{opt}(x_3) = x_3 \frac{P_{C_{x1}}\, P_{D_{x1}} \tan\left(\frac{\pi}{2\, P_{C_{x1}}}\right)}{P_{B_{x1}}} \quad (33)$$

The road type (32) defines the characteristics of the tire-road adhesion curve. The slip error (30) is defined as the difference between the current slip (κ') and the optimum slip, which is the slip that generates the maxium force. The optimum slip is obtained from the tire model equations (33), taking into account the road type. In addition, the error derivative (31) is also

defined. These values define the current operating position and how fast the system is moving with respect to the optimum value. Both values are inputs to the FLC. The FLC output is a multiplier factor (y_1), which is used to perform continuous brake pressure control. This controller is integrated in the control scheme proposed below, as shown in Fig. 5.

According to the previous description, a Mamdani type FLC is designed.The FLC has 3 inputs and only one output. The rules [23] define all possible combinations between the three inputs and the output. The algorithm optimizes the weight of each rule. If the optimized value is close to 1, it means that that rule has great relevance in the controller performance. On the contrary, if the weight value is close to 0, it means that that rule is not relevant. This way, the optimization algorithm discards the rules that are not necessary.

Restrictions are imposed to the rules to warrant system stability. Membership functions (MF) [46][47][48] are distributed throughout the Universe of Discourse interspersed by equi-spaced zones. A total of 5 MF for each input or output, either trapezoidal or triangular. These types of MF have been chosen this way because their parameterization allows them to be distributed throughout the Universe of Discourse (UoD) in an overlapping way, thus avoiding undefined input values. The following section presents the algorithm proposed to optimize the rules and MFs.

V. Coevolutionary FLC optimization

In order to minimize the number of simulations to be performed, an optimization methodology based on coevolution using genetic algorithms is proposed in this work. In this approach, two species evolve to improve the performance of the FLC. This algorithm tests the controllers on different road conditions to find the value of the parameters that define the best controller in any scenario.

Hillis et al. [49] introduced the coevolution algorithm inspired by the evolution of biological systems, preventing the system from sticking at a local maximum.

Lipson et al. [34], on the basis of the previous idea, proposed an evolutionary algorithm with two stages of exploration and estimation for a competitive coevolution. The estimation of the first species (prey) learns how to achieve a goal. Later, in the exploration stage, the second species (predator) evolves, trying to hinder the goal of the first species. This way, it is not necessary to optimize the first species to fulfill all the possible goals, since the second species looks for the weaknesses of the first one.

Hillis and Lipson developed optimization algorithms based on coevolution. These algorithms were applied to evolve systems that did not change their dynamics thorought the simulation. Instead of optimizing the design and analysis of physical systems in a fixed environment, this paper resorts to coevolution to perform the optimization of the controller of a dynamic system in a changing environment. Therefore, in this application, the dynamics of the physical system changes during the simulation.

In this approach, the estimation and exploration stages resort to binomial crossover, mutation and differential evolution strategies to generate new populations based on the results obtained by each member of the population that constitutes the species.

In an iterative way, the evolution of both species is alternated in order to obtain an FLC capable of facing any road condition without the need to simulate all the conditions in each iteration.

A. Coevolution scheme

The coevolution process is described next. The stages that require the coevolutionary algorithm are shown in Fig.6. These stages are explained in the following subsections.

1) Initialization

The number of iterations to be performed is set. Each iteration is defined as the evolution of both species sequentially. Estimation and exploration phases follow each other until the condition of the termination phase is fulfilled. The first iteration starts with a random road value.

2) Estimation

From a test defined by the road condition in the exploration phase, the estimation population evolves to achieve an FLC with improved results for that road. A chromosome represents each member of the population. This chromosome encodes the rules and MF that allow the construction of the fuzzy, as shown in Fig. 7. Different methodologies have been proposed in

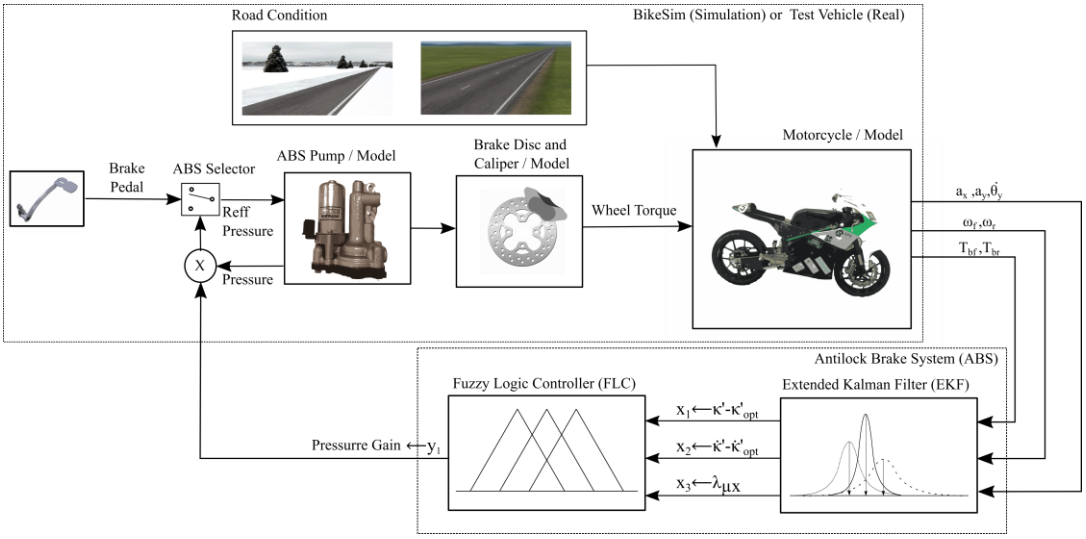

Fig. 5. Fuzzy logic controller antilock brake system block diagram

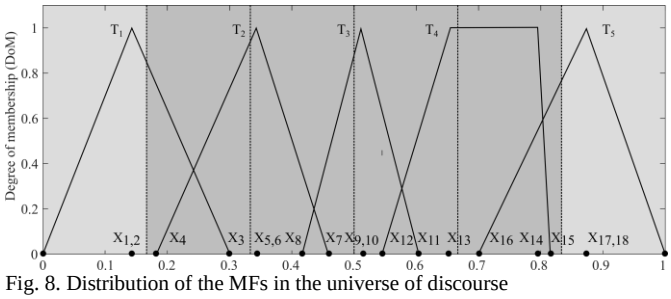

Fig. 8. Distribution of the MFs in the universe of discourse

literature to encode FLC to simultaneously optimize rules and MF. The Michigan methodology [50][51] states that each individual in the population represents a different MF and that all together constitute the FLC. On the other hand, according to the Pittsburgh method [52], each individual in the population codes a different FLC. There are also other mixed or iterative approaches [31] .

This work follows the Pittsburgh method, where each member codes an FLC using a chromosome with four sets of data. The first (R) encodes the rules, the second the weights (W), the third the type of MF (T) and the fourth the parameters of each MF (X).

a) FLC configuration

As indicated above, an FLC with 3 inputs and one output has been used, each of which consists of 5 MFs. A total of 125 rules are optimized. These rules arise from the combination of the 5 MFs of the 3 inputs with the MF of the output. There are also 125 weights associated with each of these rules (n = m = 125).

MFs of both the inputs and the output are also optimized. To do so, the range of each variable is divided equally into 6 parts, forcing the MFs to overlap in the 4 central sections. In addition, the first and last MF are fixed at the extreme ends. This way, the UoD for inputs and outputs is always defined, avoiding discontinuities on the control surface.

Each MF is defined by 4 values, except the MFs located in the extremes that are defined by 3 values, since one of them is fixed to the extreme of the UoD. This requires a total of 18 parameters (Fig. 8) for each MF, making up 72 parameters for all inputs and outputs (q=72). Each MF is associated with a triangular or trapezoidal function (p=20). In the case of the triangular MF, the central point is calculated as the average of the two central points. Both rules and MFs comprise a total of 342 parameters to be optimized (n + m + p + q) by the genetic algorithm.

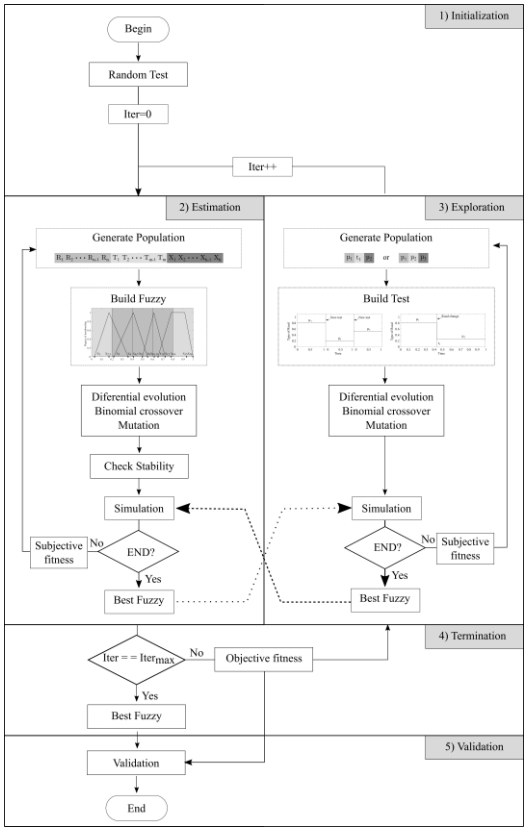

Fig. 6. Coevolutionary algorithm scheme

b) Stability Analysis

Since the FLC is very flexible in its configuration, the stability has to be analyzed before the simulation is performed.

Therefore, FLCs are discarded if they do not meet the stability requirements. A stability analysis [53] according to Lyapunov is used in order to translate the stability conditions to the rules [54]. Equation (34) is chosen as a candidate Lyapunov function.

$$V(\boldsymbol{x}) = \frac{1}{2}x_1^2 + \frac{1}{2}x_2^2 \tag{34}$$

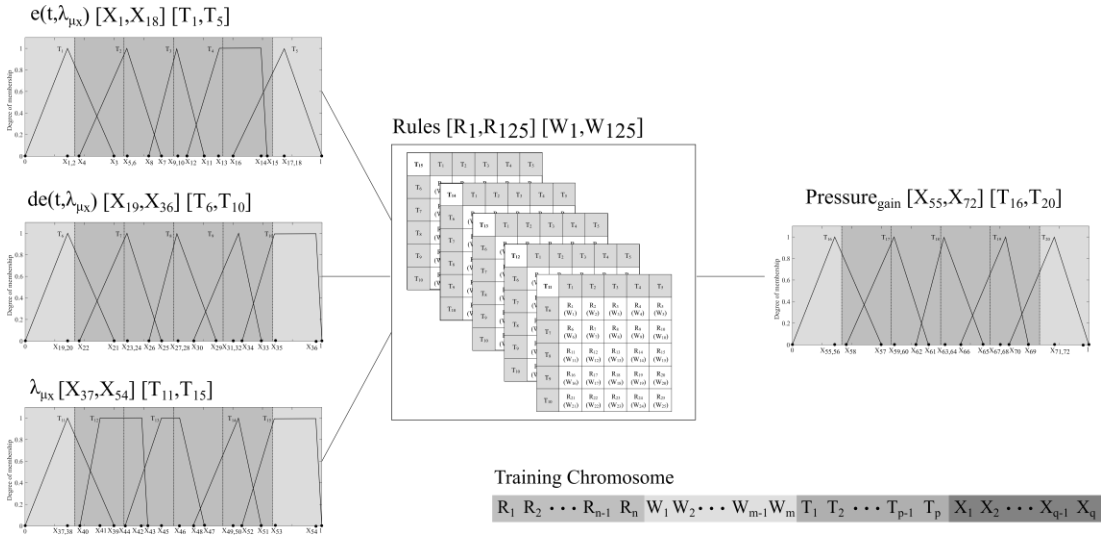

Fig. 7. Determination of the fuzzy logic from the estimation chromosome

$$\begin{cases} (1) & V(\boldsymbol{x}) = 0 \; if \; and \; only \; if \; \boldsymbol{x} = 0 \\ (2) & V(\boldsymbol{x}) > 0 \; if \; and \; only \; if \; \boldsymbol{x} \neq 0 \\ (3) & \dot{V}(\boldsymbol{x}) = \frac{d}{dt}V(\boldsymbol{x}) < 0 \; for \; all \; values \; of \; \boldsymbol{x} \neq 0 \end{cases} \quad (35)$$

According to Lyapunov, the proposed function has to satisfy (35) to ensure system stability. Before the stability analysis of the system is carried out, the following information is extracted from previous knowledge:

- The main state variables are x_1 and x_2 ($\boldsymbol{x} = (x_1, x_2)^\Gamma \in \mathbb{R}^2$). $(0,0)^\Gamma$ being a stable point.
- $\dot{x}_2$ is proportional to y_1. This is obtained from the proportional association between $\dot{x}_2$ and $\dot{T}_b$, i.e., if one increases the other one also increases and vice versa. Where T_b is the braking torque on the wheel to be controlled and $\dot{T}_b = dT_b/dt$. The braking torque and the control action y_1 are related by (36).

$$\dot{x}_2 \propto \dot{T}_b = y_1 T_b - T_b = (y_1 - 1)T_b \quad (36)$$

The three conditions described in (35) are analyzed below to ensure system stability:

1. The first condition is met according to the proposed function (37).
$$V(\boldsymbol{x} = \boldsymbol{0}) = V((0,0)^\Gamma) = \tfrac{1}{2}0^2 + \tfrac{1}{2}0^2 = 0 \quad (37)$$
2. The second condition is fulfilled $\forall \, \boldsymbol{x} \neq 0$ since the function used is quadratic (38).
$$V(\boldsymbol{x} \neq \boldsymbol{0}) = V((x_1, x_1)^\Gamma \neq (0,0)^\Gamma) = \tfrac{1}{2}x_1^2 + \tfrac{1}{2}x_2^2 > 0 \quad (38)$$
3. The third stability condition is proven by analyzing the derivative of the proposed function (39).
$$\dot{V}(\boldsymbol{x}) = x_1\dot{x}_1 + x_2\dot{x}_2 = x_1x_2 + x_2\dot{x}_2 < 0 \quad (39)$$
This condition yields 4 possible requirements (40) to assure stability.
$$\begin{cases} (x_1 > 0) \,\&\, (x_2 < 0) \,\&\, (x_1x_2 < 0) \longrightarrow \dot{x}_2 = 0 \\ (x_1 < 0) \,\&\, (x_2 > 0) \,\&\, (x_1x_2 < 0) \longrightarrow \dot{x}_2 = 0 \\ (x_1 > 0) \,\&\, (x_2 > 0) \longrightarrow \dot{x}_2 < -x_1 \\ (x_1 > 0) \,\&\, (x_2 > 0) \longrightarrow \dot{x}_2 > -x_1 \end{cases} \quad (40)$$

These requirements are translated to the FLC (41). In addition, it is taken into consideration that $|\dot{x}_2| > |x_1| \; \forall \, \boldsymbol{x} \neq 0$ due to system characteristics.

$$\begin{cases} (x_1 > 0) \,\&\, (x_2 > 0) & \longrightarrow & y_1 < 1 \\ (x_1 < 0) \,\&\, (x_2 < 0) & \longrightarrow & y_1 > 1 \\ (x_1 \geq 0) \,\&\, (x_2 < 0) & \longrightarrow & y_1 = 1 \\ (x_1 < 0) \,\&\, (x_2 \geq 0) & \longrightarrow & y_1 = 1 \end{cases} \quad (41)$$

3) Exploration

This phase starts from the best FLC of the estimation stage and, through evolution of the population, seeks a road condition for which it obtains the worst subjective fitness. Therefore, it is shown that the estimation stage tries to minimize subjective fitness while the exploration stage focuses on maximizing it.

The exploration population encodes the tests using a chromosome that can be defined in two different ways (see Fig. 9). The first option is a test in which three consecutive simulations are performed on three different roads. These roads are coded in the chromosome according to ($\lambda_{\mu x,1}$, $\lambda_{\mu x,2}$, $\lambda_{\mu x,3}$). The second option is a test with only one simulation that starts with a road condition ($\lambda_{\mu x,1}$) and, after given time t_1, changes to a different road ($\lambda_{\mu x,2}$). The first type of coding, ($\lambda_{\mu x,1}$, $\lambda_{\mu x,2}$, $\lambda_{\mu x,3}$), presents a faster convergence but requires a higher computational cost. On the other hand, in the case of road change ($\lambda_{\mu x,1}$, t_1 , $\lambda_{\mu x,2}$), the computational cost is lower but, due to the transient component of the fitness equation, it accumulates a higher error, which reduces the convergence rate. The first method is selected to take advantage of its faster convergence.

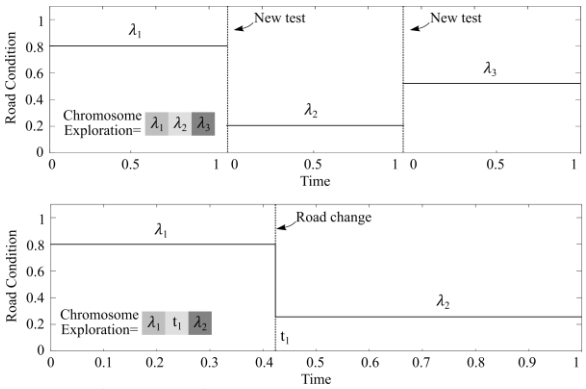

Fig. 9. Test configuration of exploration chromosome

4) Termination

The optimization process is repeated until the predefined number of iterations is reached.

5) Validation

Once the optimization algorithm finishes, the convergence of the objective and subjective fitness functions are analyzed. The value of both functions should decrease as the number of iterations increases. This way, the value decreases fast during the first iterarions. However, when the process goes forward, the rate of improvement slowly reduces until a certain number of iterations. Beyond this number of iterations, the value of the fitness function oscillates and the performances of the generated FLCs are not improved. This is common behavior found in coevolutionary approaches. The FLC that has obtained the best subjective fitness in all iterations is the output of the coevolution process.

B. Fitness Function

In order to evaluate each member of the population, a subjective and an objective fitness are defined. The first one evaluates the performance of the individual in a given road condition. This subjective fitness is calculated in each iteration, being particular in each case, and does not reflect how the algorithm evolves globally. The objective fitness evaluates the global performance of the individual from a road sweep ($\lambda_{\mu x} = \{0.4\,;\, 0.5\,;\, 0.6\,;\, 0.7\,;\, 0.8\}$). The objective fitness does not affect the evolution and, in order to reduce computational cost, it is only calculated each time the species is changed.

The fitness function (η) (42) evaluates the result obtained by each FLC for a given test. It is calculated on the basis of two parameters: the mean deceleration, $\overline{a_x}$, and the mean of the slip error ($\bar{e} = \overline{x_1}$). In order to obtain a dimensionless parameter, the mean deceleration is divided by the maximum deceleration obtained according to equation (43). The minimum value between the maximum tire grip and the limit stoppie grip determined by the geometry of the vehicle is taken into consideration. Secondly, the slip error obtained during the test is used to prevent the wheel from locking.

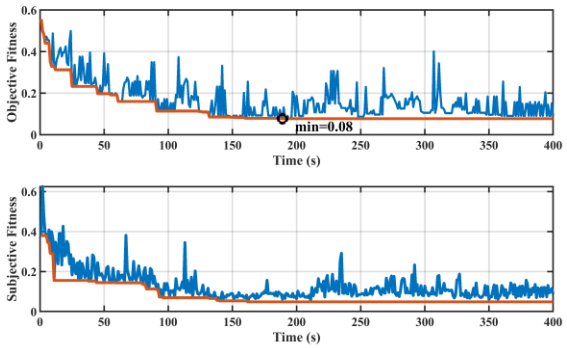

Fig. 10. Objective and subjective fitness.

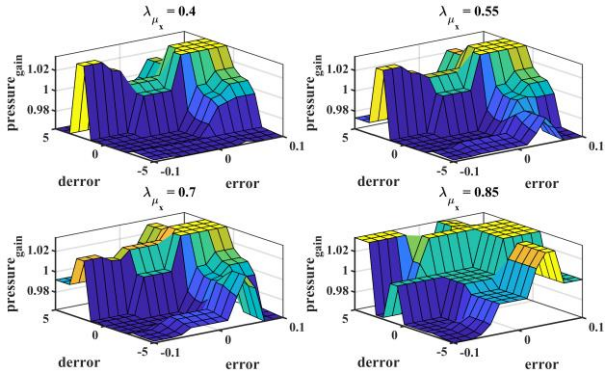

Fig. 11. Control surface for different road conditions

$$\eta(e, a_x, \lambda_{\mu x}) = \bar{e} + \frac{\overline{a_x}}{a_{x,max}(\lambda_{\mu x})} \tag{42}$$

$$a_{x,max}(\lambda_{\mu x}) = \begin{cases} g \min\left(\frac{L_f}{z}, \lambda_{\mu_x} P_{D_{x1}}\right) & T_{bf} > 0;\ T_{br} > 0 \\ g \min\left(\frac{Lf}{z}, \frac{L_r \lambda_{\mu_x} P_{D_{x1}}}{L_r + L_f}\right) & T_{bf} > 0;\ T_{br} = 0 \\ g \frac{L_f}{L_r + L_f} \lambda_{\mu_x} P_{D_{x1}} & T_{bf} = 0;\ T_{br} > 0 \end{cases} \tag{43}$$

Remark 4: Coevolution allows reducing the number of simulations compared to a simple genetic algorithm. The exploration stage enables the algorithm to rapidly find the worst case scenario in a reduced number of simulations. Therefore, the algorithm focuses on improving the performance in this scenario rather than in all possible ones.

VI. Results

Results obtained from simulations and real experiments are presented in this section. The performance of the optimized controller was tested by conducting brake tests on different surfaces. Due to safety reasons, only rear braking tests were carried out. For comparison reasons, simulations were also perfomed using only the rear brake. Initial vehicle speed was set at 40 km/h and final speed was 10 km/h. Table II shows the deceleration achieved in simulations and real tests with the proposed controller and a conventional ABS [1][55].Best performance was obtained with the proposed controller in simulations as well as in real tests. No wheel locking was observed in any case.

A. Simulation

The total number of iterations in the optimization process is set at 400. The estimation and exploration populations consist of 30 and 10 individuals respectively. The results obtained for objective and subjective fitness are presented in Fig. 10.

It is observed that during the first 200 iterations, convergence is fast, with the minimum subjective error found in iteration number 162. After that iteration, the algorithm keeps searching for a better solution. However, the value of the fitness function oscillates without improving the overal result. As mentioned before, this behaviour is commonly observed in optimization processes based on coevolutionary approaches. Fig.11 reproduces the control surface for four road conditions. The control surface maintains a constant working area for all roads. However, surface differences are observed for negative x_2. This is due to the fact that the dynamics of the system become faster as the adherence increases, so the slopes in these cases must be reduced. The results obtained by simulation in BikeSim® for different road conditions are presented in Fig. 12-16.

1) Dry Road ($\lambda_{\mu x} = 1.1$)

As mentioned above, as grip increases, the system becomes more unstable and faster, causing speed and pressure oscillations (Fig.12). In addition, as seen in vertical force F_z, the load transfer is higher, which reduces rear braking force F_x. Despite this fact, the estimation is appropriate.

2) Wet Road ($\lambda_{\mu x} = 0.9$)

The simulation presents the same behavior as on a dry road. However, lower pressures are required for lower adherence surfaces (Fig.13).

3) Low Friction Road ($\lambda_{\mu x} = 0.65$)

The dynamics of the braking process on a low-grip road is slow, causing fewer oscillations throughout the simulation (Fig.14). Again, the estimation of the road condition is adequate. Likewise, the pressure setpoint applied to the rear wheel remains quite constant during the simulation, with the adjustments of the FLC being small.

4) Road Change

The FLC is tested for variations in the road condition: low-dry Fig.15 and dry-low Fig.16. The surface change takes place after 1 s. of simulation. It is checked how, during the change of road, the controller quickly adapts to the slip ratio associated with the optimum value of the new surface. The estimation of the road condition during this transient process, due to the rapid change

TABLE II
Simulation and Test Results

Road	FLC – Bikesim Deceleration (g_s)	Conv. – Bikesim Deceleration (g_s)	FLC – Real Test Deceleration (g_s)	Conv. – Real Test Deceleration (g_s)
Dry	**0.356**	**0.356**	**0.351**	0.348
Wet	**0.326**	0.323	**0.320**	0.314
Low	**0.240**	0.238	**0.238**	0.223
Low-Dry	**0.290**	0.264	-	-
Dry-Low	**0.277**	0.249	-	-

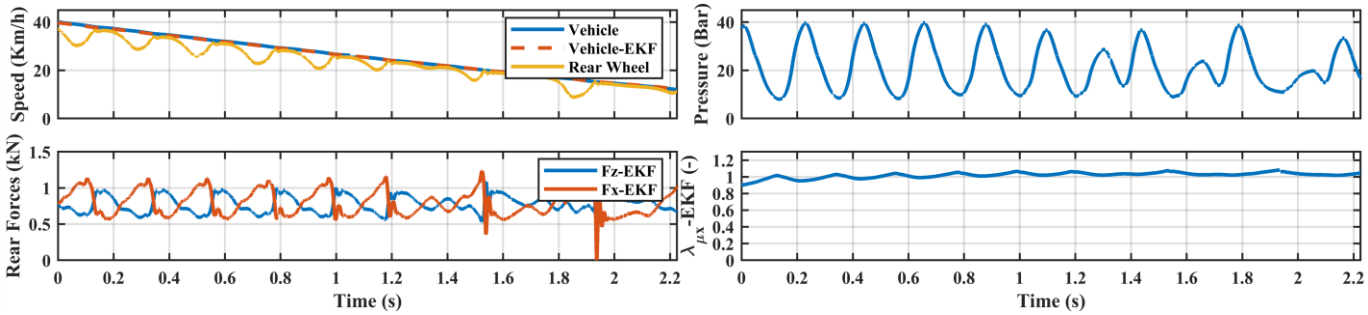

Fig. 12. Dry road ($\lambda_{\mu x}$=1.1) simulation results

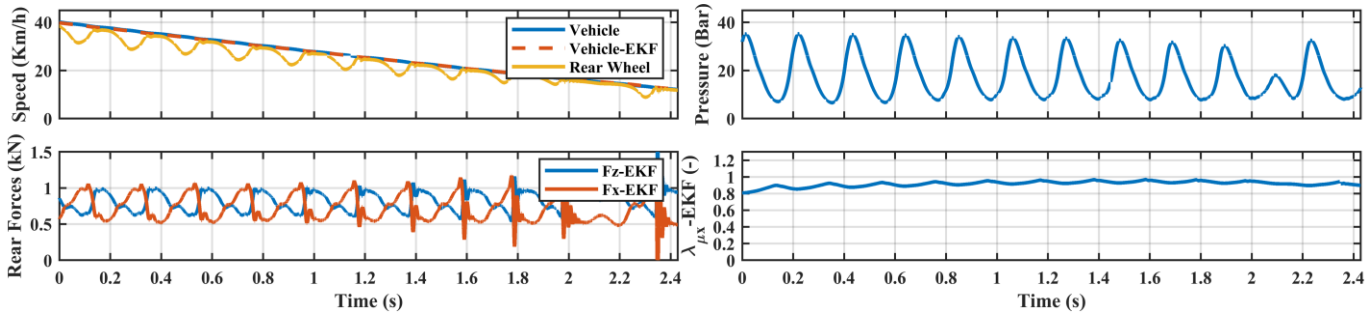

Fig. 13. Wet road ($\lambda_{\mu x}$=0.9) simulation results

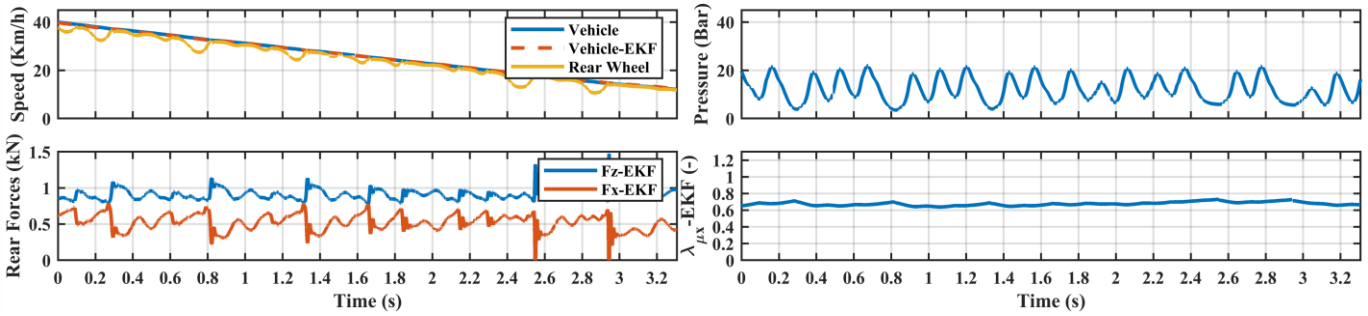

Fig. 14. Low friction road ($\lambda_{\mu x}$=0.65) simulation results

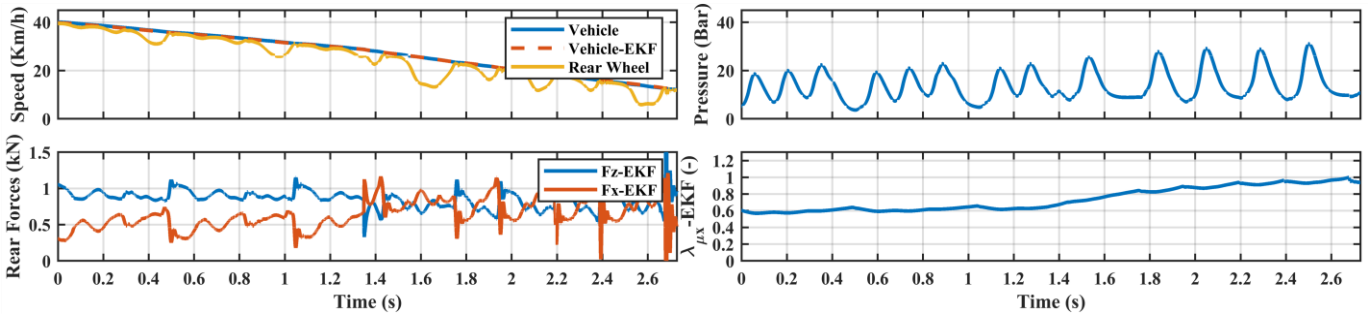

Fig. 15. Low-Dry road change simulation results

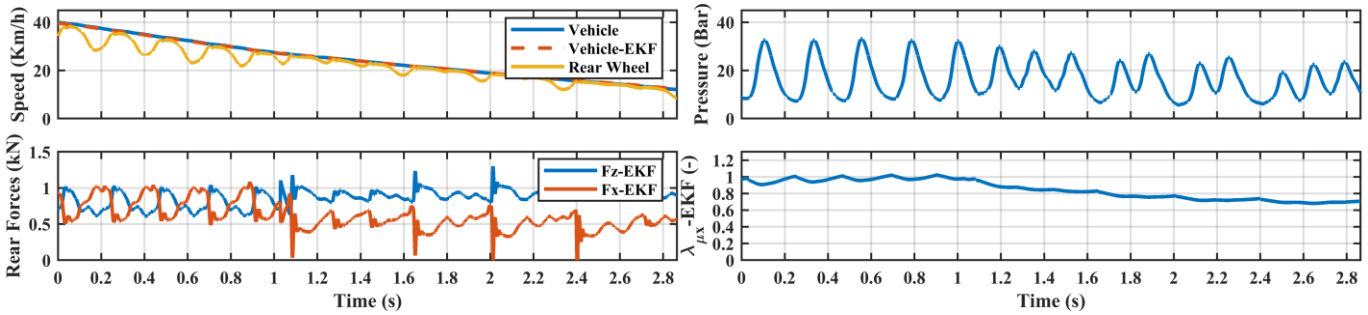

Fig. 16. Dry-Low road change simulation results

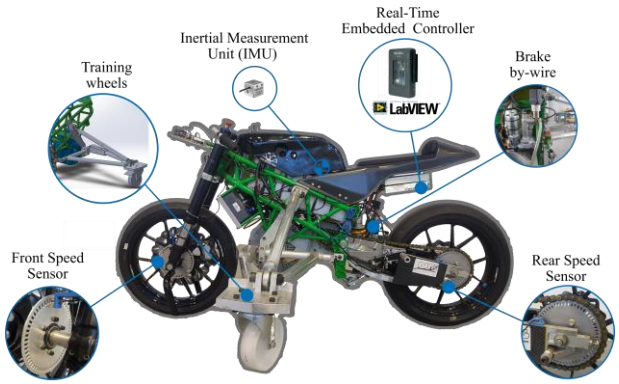

Fig. 17. Test vehicle

in the forces of tire-road interaction, requires an adaptation time to converge to the new value. Nevertheless, the FLC adapts to the surface without causing large slips during the transient process.

B. *Experimentation*

In order to validate the optimization of the FLC, several tests were carried out on a real vehicle. The real vehicle shown in Fig. 17 was equipped with a myRIO real-time embedded controller running the proposed ABS FLC. In addition, speed sensors were installed on the front and rear wheels as well as a by-wire brake on the rear wheel, an inertial measurement unit (IMU) and training wheels for safety reasons.

1) *Dry Road*

A similar response to the simulation is observed with the same deceleration rates (Fig.18 and Table II). Futhermore, it can be seen that the oscillations in pressure and wheel speeds are similar to those obtained in the simulations.

2) *Wet Road*

Due to the porosity of the asphalt, the grip does not drop significantly (Fig.19). Pressure fluctuations are slightly higher compared to the simulation, but the same level of slips are obtained.

3) *Low Friction Road*

In the case of a lower grip road, mismatches of optimal slip provided by the tyre model have a big influence on the response of the controller. This makes it impossible for the controller to maintain the slip ratio as properly as it does in the simulation (Fig.20). However, the performance of the controller is considered to be satisfactory even in low adherence conditions. Further improvements will be achieved if the tyre models are modified to provide an optimal slip closer to reality in low adherence conditions.

Even though simulation and experimentation share parameters (Table III), some discrepancies can be observed between simulation and experimental results. A more oscillatory controller output is observed in the real tests. This way, measured pressure fluctuations are slightly higher compared to the simulation. However, similar slip rates and deceleration levels are obtained in both cases (Table II). This fact can be attributed to the parameters used in the tire model and system component modelling inaccuracies. In the first case, surface,

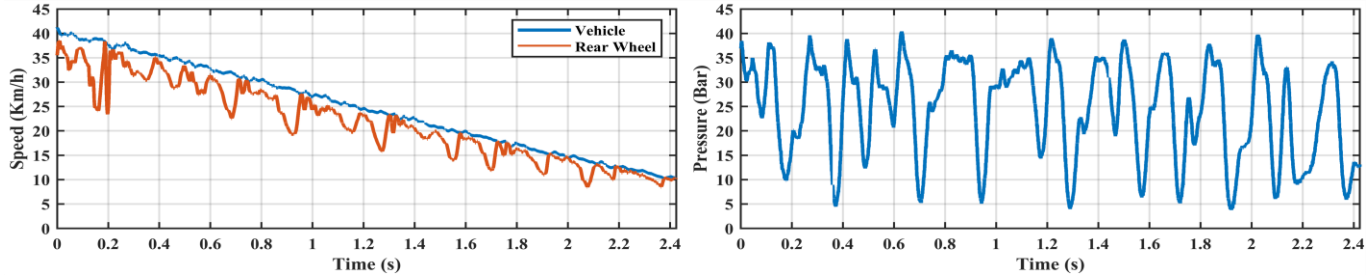

Fig. 18. Dry road real test results

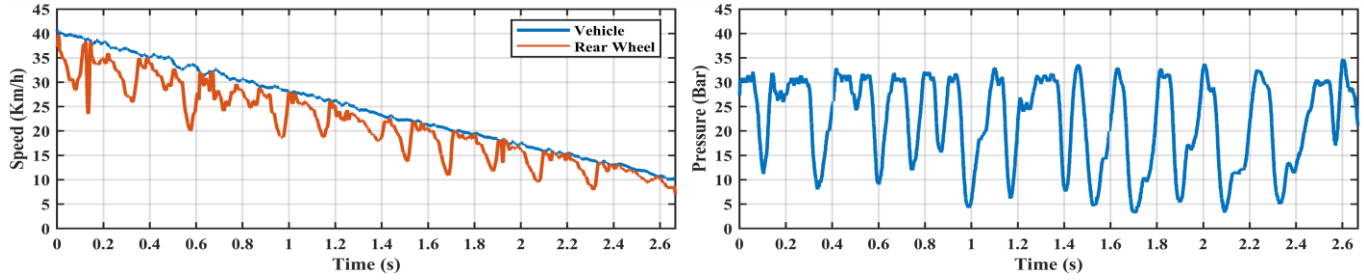

Fig. 19. Wet road real test results

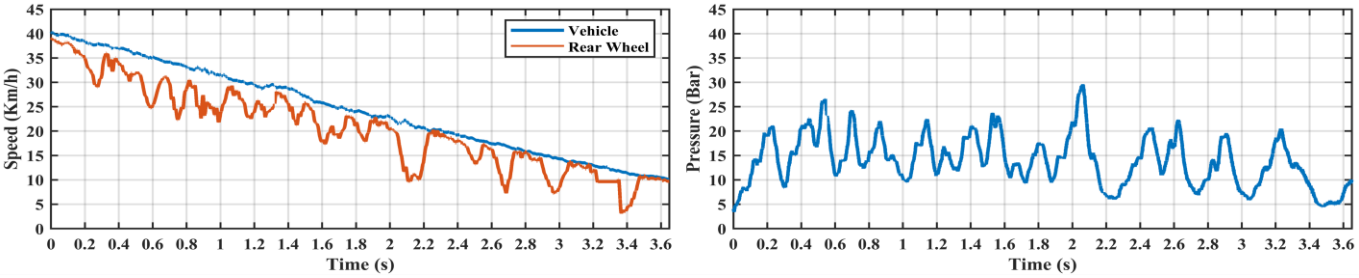

Fig. 20. Low friction road real test results

temperature, water film depth and tire parameters can influence the obtained results. In the second case, real systems may require more complex models to reproduce their behavior, such as may happen with the brake pad – brake disk contact.

Remark 5: For safety reasons, the proposed controllers were implemented only in the rear axle in the experimental vehicle. Due to this fact, simulations were performed using only the rear axle too. This way, it was possible to perform fair comparisons. The proposed methodology can be applied to the two wheels of a motorcycle or to 4-wheeled vehicles by using the adequate system equations.

TABLE III
SIMULATION AND EXPERIMENT PARAMETER VALUES

Symbol	Value	Symbol	Value
M	190 kg	F_{z0}	1100 N
CoG (x,z)	(0,0.550) m	P_{Bx}	25.939
R_f	0.282 m	P_{Cx}	1.606
R_r	0.297 m	P_{Dx}	1.380
L_f	0.552 m	P_{Ex}	0.026
L_r	0.740 m	σ_κ	0.025 m
I_y	7.34 kg m^2	R	2.85 Ω
I_{wf}	0.484 kg m^2	L	0.050 H
I_{wr}	1.298 kg m^2	K_t	23.13 bar/A
K_f	25 N/mm	τ_{up}	0.061 s
K_r	40 N/mm	τ_{down}	0.083 s
C_r	2 N s/mm	S_p	2300 mm^2
C_f	10 N s/mm	μ_p	0.4
L_0	1182 N	ϕ_d	196 mm
C_d	0.188 kg/m	Δt	1 ms

VII. CONCLUSION

A coevolutionary-based algorithm has been developed to optimize Fuzzy Logic Controllers for anti-lock brake systems. This algorithm is based on improving the performance of the ABS controller under changing road conditions. Coevolution speeds up the optimization process by taking into account the worst-case scenarios. This reduces the computational cost of the FLC optimization process significantly, as it avoids simulations where the FLC already works properly.

The temporal response of the brake system components and the delays in the measurements and estimation processes are taken into account in the models used by the optimization algorithms. This way, the model reproduces the real system with greater fidelity. This methodology contributes to a faster implementation of the proposed controllers in real applications. Simulations have been carried out to evaluate the performance of the solution provided by the optimization algorithm. Furthermore, the proposed FLC has been tested in real conditions using a two-wheel electric vehicle. Its performance has been compared to a conventional controller used in commercial vehicles. Results show the superior performance of the proposed FLC in all scenarios.

Future research will consider the modelling of the lateral behavior of the motorcycle in the simulation models used by the optimization algorithm. In addition, a modified tire model will be considered to take into account different road surfaces and combined longitudinal and lateral tire forces.

REFERENCES

[1] Reif, K. “Antilock braking system (ABS),” in *Brakes, Brake Control and Driver Assistance Systems*, 1st ed. Friedrichshafen, Germany: Springer Vieweg, 2014, pp 74-93.

[2] G. F. Mauer, “A fuzzy logic controller for an ABS braking system,” *IEEE T. Fuzzy Syst.*, vol. 3, no. 4, pp. 381-388, Nov. 1995.

[3] V. Ivanov, D. Savitski and B. Shyrokau, “A Survey of Traction Control and Antilock Braking Systems of Full Electric Vehicles With Individually Controlled Electric Motors,” *IEEE Transactions on Vehicular Technology*, vol. 64, no. 9, pp. 3878-3896, Sept. 2015.

[4] Sharkawy, A. B. “Genetic fuzzy self-tuning PID controllers for antilock braking systems”. *Engineering Applications of Artificial Intelligence*, vol. 23, no 7,pp. 1041–1052, 2010.

[5] C. Lin and H. Li, “Intelligent Hybrid Control System Design for Antilock Braking Systems Using Self-Organizing Function-Link Fuzzy Cerebellar Model Articulation Controller,” *IEEE Transactions on Fuzzy Systems*, vol. 21, no. 6, pp. 1044-1055, Dec. 2013.

[6] P. Khatun, C. M. Bingham, N. Schofield and P. H. Mellor, “Application of fuzzy control algorithms for electric vehicle antilock braking/traction control systems,” *IEEE Transactions on Vehicular Technology*, vol. 52, no. 5, pp. 1356-1364, Sept. 2003.

[7] T. Shim, S. Chang and S. Lee, “Investigation of Sliding-Surface Design on the Performance of Sliding Mode Controller in Antilock Braking Systems,” *IEEE Transactions on Vehicular Technology*, vol. 57, no. 2, pp. 747-759, March 2008.

[8] Poursamad, A. “Mechatronics Adaptive feedback linearization control of antilock braking systems using neural networks,” *Mechatronics*, vol. *19*, no. 5,pp. 767–773, 2009.

[9] W. Sun, J. Zhang and Z. Liu, “Two-Time-Scale Redesign for Antilock Braking Systems of Ground Vehicles,” *IEEE Transactions on Industrial Electronics*, vol. 66, no. 6, pp. 4577-4586, June 2019.

[10] K. Han, B. Lee and S. B. Choi, “Development of an Antilock Brake System for Electric Vehicles Without Wheel Slip and Road Friction Information,” *IEEE Transactions on Vehicular Technology*, vol. 68, no. 6, pp. 5506-5517, June 2019.

[11] Mustafa, G. I. Y., Wang, H. P., & Tian, Y. “Advances in Engineering Software Vibration control of an active vehicle suspension systems using optimized model-free fuzzy logic controller based on time delay estimation,” *A. Engineering Software*, vol. *127*, pp. 141–149, 2019.

[12] Li, H., Wang, X., Song, S., & Li, H. “Vehicle Control Strategies Analysis Based on PID and Fuzzy Logic Control,” *Procedia Engineering*, vol. *137*, pp. 234–243, 2016.

[13] C. Hwang, C. Yang and J. Y. Hung, “Path Tracking of an Autonomous Ground Vehicle With Different Payloads by Hierarchical Improved Fuzzy Dynamic Sliding-Mode Control,” *IEEE T. Fuzzy Syst*, vol. 26, no. 2, pp. 899-914, April 2018.

[14] N. Wang, S. Su, J. Yin, Z. Zheng and M. J. Er, “Global Asymptotic Model-Free Trajectory-Independent Tracking Control of an Uncertain Marine Vehicle: An Adaptive Universe-Based Fuzzy Control Approach,” *IEEE Transactions on Fuzzy Systems*, vol. 26, no. 3, pp. 1613-1625, 2018.

[15] Shiuh-Jer Huang and Wei-Cheng Lin, “Adaptive fuzzy controller with sliding surface for vehicle suspension control,” IEEE Transactions on Fuzzy Systems, vol. 11, no. 4, pp. 550-559, Aug. 2003.

[16] Zhang, J., Wang, H., Zheng, J., Cao, Z., Man, Z., Yu, M., & Chen, L. “Adaptive Sliding Mode-based Lateral Stability Control of Steer-by-Wire Vehicles with Experimental Validations”. *IEEE Transactions on Vehicular Technology*, 9545(c), 1–1, 2020.

[17] Ye, M., & Wang, H. “A Robust Adaptive Chattering-Free Sliding Mode Control Strategy for Automotive Electronic Throttle System via Genetic Algorithm”. *IEEE Access*, 8, 68–80, 2020.

[18] Wang, H., He, P., Yu, M., Liu, L., Do, M. T., Kong, H., & Man, Z. “Adaptive neural network sliding mode control for steer-by-wire-based vehicle stability control”. *Journal of Intelligent and Fuzzy Systems*, 31(2), 885–902, 2016.

[19] Pacejka, H. B. “Applications of transient tyre models,” in *Tyre and Vehicle Dynamics*, 3rd ed. Oxford, UK: Butterworth-Heinemann, 2007, pp. 364–411.

[20] Burckhardt, M.. *Fahrwerktechnik: Radschlupf Regelsysteme*. Würzburg, Germany: Vogel-Verlag. 1st ed.1993.

[21] Pérez, J., & Santos, M. “Fuzzy logic steering control of autonomous vehicles inside roundabouts”. *Applied Soft Computing*, vol. *35*, pp. 662–669, 2015.

[22] L. Wang and J. M. Mendel, “Generating fuzzy rules by learning from examples,” *IEEE Transactions on Systems, Man, and Cybernetics*, vol. 22, no. 6, pp. 1414-1427, Nov.-Dec. 1992.
[23] Yuhui Shi, R. Eberhart and Yaobin Chen, “Implementation of evolutionary fuzzy systems,” *IEEE T. Fuzzy Syst*, vol. 7, no. 2, pp. 109-119, April 1999.
[24] C. Perneel, J. -. Themlin, J. -. Renders and M. Acheroy, “Optimization of fuzzy expert systems using genetic algorithms and neural networks,” *IEEE T. Fuzzy Syst*, vol. 3, no. 3, pp. 300-312, Aug. 1995.
[25] I. Baturone, F. J. Moreno-Velo, S. Sanchez-Solano and A. Ollero, “Automatic design of fuzzy controllers for car-like autonomous robots,” *IEEE T. Fuzzy Syst*, vol. 12, no. 4, pp. 447-465, Aug. 2004.
[26] Mohammadi, E., & Montazeri-gh, M. “A fuzzy-based gas turbine fault detection and identification system for full and part-load performance deterioration,” *Aerospace Science and Technology*, vol. *46*,pp. 82–93, 2015.
[27] Gola, A., & Kłosowski, G. “Development of computer-controlled material handling model by means of fuzzy logic and genetic algorithms,”*Neurocomputing*, vol. 330, April,2019.
[28] M. Collotta, G. Pau and V. Maniscalco, “A Fuzzy Logic Approach by Using Particle Swarm Optimization for Effective Energy Management in IWSNs,” *IEEE Transactions on Industrial Electronics*, vol. 64, no. 12, pp. 9496-9506, Dec. 2017.
[29] R. P. Prado, S. Garcia-Galán, J. E. M. Exposito and A. J. Yuste, “Knowledge Acquisition in Fuzzy-Rule-Based Systems With Particle-Swarm Optimization,” *IEEE T. Fuzzy Syst*, vol. 18, no. 6, pp. 1083-1097, Dec. 2010.
[30] Cabrera, J. A., Estebanez, B., Nadal, F., & Simon, A. “A coevolutionary algorithm for tyre model parameters identification,” *Structural and Multidisciplinary Optimization*, vol.41,no. 5, pp. 749–763, 2010.
[31] C. A. Pena-Reyes and M. Sipper, "Fuzzy CoCo: a cooperative-coevolutionary approach to fuzzy modeling," in IEEE Transactions on Fuzzy Systems, vol. 9, no. 5, pp. 727-737, Oct. 2001.
[32] J. Fan, J. Wang and M. Han, “Cooperative Coevolution for Large-Scale Optimization Based on Kernel Fuzzy Clustering and Variable Trust Region Methods,” *IEEE T. Fuzzy Syst*, vol. 22, no. 4, pp. 829-839, 2014.
[33] Kwee-Bo Sim, Kwang-Sub Byun and Dong-Wook Lee, “Design of fuzzy controller using schema coevolutionary algorithm,” *IEEE Transactions on Fuzzy Systems*, vol. 12, no. 4, pp. 565-570, Aug. 2004.
[34] Lipson, H., Bongard, J., & Zykov, V. (2005). Coevolutionary methods in systems design and analysis.Presented at 15th international CIRP design seminar. Shanghai, China
[35] He, Q. & Ã, L. W. “An effective co-evolutionary particle swarm optimization for constrained engineering design problems,” *Engineering Applications of Artificial Intelligence*, vol. *20*, pp. 89–99, 2007.
[36] M. Antonelli, P. Ducange and F. Marcelloni, “Genetic Training Instance Selection in Multiobjective Evolutionary Fuzzy Systems: A Coevolutionary Approach,” *IEEE Transactions on Fuzzy Systems*, vol. 20, no. 2, pp. 276-290, April 2012.
[37] J. A. Cabrera, J. J. Castillo, E. Carabias and A. Ortiz, “Evolutionary Optimization of a Motorcycle Traction Control System Based on Fuzzy Logic,” *IEEE T. Fuzzy Syst*, vol. 23, no. 5, pp. 1594-1607, Oct. 2015.
[38] R.S. Sharp, S. E. and D. J. N. L. “Advances in the Modelling of Motorcycle Dynamics". *Multibody System Dynamics*, vol. 12, no. 1, pp. 251–283. 2004.
[39] Z. Zhang, L. Wang, J. Zhang and R. Ma, “Study on Requirements for Load Emulation of the Vehicle With an Electric Braking System,” IEEE Transactions on Vehicular Technology, vol. 66, no. 11, pp. 9638-9653, Nov. 2017.
[40] T. Goggia et al., “Integral Sliding Mode for the Torque-Vectoring Control of Fully Electric Vehicles: Theoretical Design and Experimental Assessment,” IEEE Transactions on Vehicular Technology, vol. 64, no. 5, pp. 1701-1715, May, 2015.
[41] N. Guo, B. Lenzo, X. Zhang, Y. Zou, R. Zhai and T. Zhang, “A Real-time Nonlinear Model Predictive Controller for Yaw Motion Optimization of Distributed Drive Electric Vehicles,” IEEE Transactions on Vehicular Technology, pp. 1, 2020.
[42] Taylor, P., Cheng, C., & Cebon, D. “Dual extended Kalman filter for vehicle state and parameter estimation”. Vehicle System Dynamics: International Journal of Vehicle Mechanics and Mobility, 2010.
[43] T. A. Wenzel, K. J. Burnham, M. V. Blundell & R. A. Williams “Dual extended Kalman filter for vehicle state and parameter estimation”, Vehicle System Dynamics,vol. 44, no.2, pp. 153-171,2006
[44] Rajamani, R.; Piyabongkarn, D.; Lew, J.; Yi, K.; Phanomchoeng, G.: “Tire road friction coefficient estimation real-time estimation methods for active automotive safety applications”. *IEEE Control Systems Magazine*, , vol. 30: no. 4, pp. 54-69. 2010.
[45] W. Zhang et al., "Advanced Vehicle State Monitoring: : Evaluating Moving Horizon Estimators and Unscented Kalman Filter," *IEEE Transactions on Vehicular Technology*, vol. 68, no. 6, s. 5430-5442, 2019.
[46] Arslan, A., & Kaya, M. “Determination of fuzzy logic membership functions using genetic algorithms”. *Fuzzy Sets and Systems*, vol. *118*, pp. 297–306, 2001.
[47] Wang, D., Lin, X., & Zhang, Y. “Automation in Construction Fuzzy logic control for a parallel hybrid hydraulic excavator using genetic algorithm,” *Automation in Construction*, vol. 20, no. 5, pp. 581–587, 2011.
[48] Chen, J., Zhu, H., Zhang, L., & Sun, Y. “Research on fuzzy control of path tracking for underwater vehicle based on genetic algorithm optimization,” *Ocean Engineering*, vol. *156*, pp. 217–223, 2018.
[49] Hillis, W. D. “Co-evolving parasites improve simulated evolution as an optimization procedure”. *Physica D: Nonlinear Phenomena*, vol. *42*, pp. 228–234, 1990.
[50] Casillas, J., Carse, B., & Bull, L. Fuzzy-XCS : “A Michigan Genetic Fuzzy System. *IEEE T. Fuzzy Syst,”* vol. *15*(4), pp. 536–550, 2007.
[51] Booker, L. B., Goldberg, D. E., & Holland, J. . “Classifier systems and genetic algorithms”. *Artificial Intelligence*, vol. 40, pp. 235–282, 235–282,1989.
[52] Carse, B., Fogarty, T. C., & Munro, “A Evolving fuzzy rule based controllers using genetic algorithms,” *Fuzzy Sets and Systems*, vol. 80, no. 3, pp. 273–293, 1996.
[53] Fu, Y., Li, H., & Kaye, M. “Design and Lyapunov Stability Analysis of a Fuzzy Logic Controller for Autonomous Road Following,” *Mathematical Problems in Engineering*,vol., 2010.
[54] Margaliot, M., & Langholz, G. “Fuzzy Lyapunov-based approach to the design of fuzzy controllers”, *Fuzzy Sets and Systems*, vol. *106*, pp. 49–59, 1999.
[55] Day, T. and Roberts, S., “A Simulation Model for Vehicle Braking Systems Fitted with ABS” *SAE Technical Paper*,2002.

Javier Pérez Fernández (Graduate Student Member, IEEE) received a B.S. and a M.S. in Industrial Engineering, from the University of Malaga, Spain.
He is studying his Ph.D. in Mechanical Engineering and is a researcher of Mechanical Engineering at the University of Malaga. His research interests include modeling and control of vehicle safety systems, electric vehicles and spiking neural networks.

Manuel G. Alcázar Vargas (Student Member, IEEE) received a B.S. in Mechanical Engineering and a M.S. in Industrial Engineering from the University of Jaén, Spain.
He is studying his Ph.D. in Mechanical Engineering and is a researcher of Mechanical Engineering at the University of Malaga. His research interests include electric vehicles and tire dynamics.

Juan M. Velasco Garcia (Student Member, IEEE) received a B.S. in Mechanical Engineering and Electronic Engineering and a M.S. in Mechatronic Engineering from the University of Malaga, Spain.
He is a researcher of Mechanical Engineering at the University of Malaga. His research interests include vehicle dynamics and parameter estimation.

Juan A. Cabrera Carrillo received a B.S. in Mechanical Engineering, a M.S. in Computer Science, and a Ph.D. Degree in Mechanical Engineering from the University of Malaga, Spain.
He is Full Professor of Mechanical Engineering at the University of Malaga. His research interests include modeling and control of vehicle safety systems and parameter estimation, advanced vehicle systems, genetic algorithms applied to synthesis of mechanisms, tire models and control systems, and spiking neural networks.

Juan J. Castillo Aguilar (Member, IEEE) received a B.S., M.S., and Ph.D. Degree in Mechanical Engineering from the University of Malaga, Spain.
He is an Associate Professor of Mechanical Engineering at the University of Malaga. His research interests include vehicle dynamics, modeling and control of vehicle safety systems, vehicle testing, optimization algorithms and parameter estimation.